A ROTOR SPEED DETECTOR FOR INDUCTION MACHINES:
THE SIGNAL PROCESSING PART

B. HÄMMERLI AND R. ZWICKY

Institute for Automatic Control and Industrial Electronics
Swiss Federal Institute of Technology
Switzerland

Abstract

A new method to detect rotor speed electrically from rotor slots harmonics of a three-phase squirrel cage induction motor fed with a 20 kHz pulse width modulated (PWM) inverter is presented. The rotor speed is detected in the range 20% to 100% of nominal speed directly by the rotor slots harmonics and in the range from 2% to 30% of nominal speed an additional 1 kHz three phase signal is fed from the inverter into the machine to produce an additional rotor-slot-modulation, which is used to detect rotor speed in this range. Principal signal detection schemes are shown. A simulation model based on current distribution in the motor is explained by signal processing methods. Practical EMC problems are discussed additionally.

Keywords: Squirrel cage induction motor, (sensorless) speed detection, PWM drive, harmonics, simulation of ASM harmonics, three phase injection.

Introduction

The work presented in this paper is concerned with conventional 1500 rpm motors with 28 rotor and 36 stator slots which are fed with a high frequency (20 kHz) transistor PWM (pulse width modulated) inverter. These drives have usually a tachogenerator or a slip compensator to detect or to stabilize the rotor speed. Of these applications there are some which do not need very high dynamic response. The objective of this work is to replace the quite expensive tachogenerator in such applications, and the following goals have been set to design the detector:

— Additional power electronics should be avoided;
— Extension of the rotor speed detectable range;
— Minimization of the processing hardware.

Early theoretical considerations (TAEGEN and HOMMES, 1972; FRANZ, 1974), based on a Fourier analysis of the current distribution in the rotor, have proposed the equations (1)-(5). The simulation of the equations needs a high performance computer (MFLOPS). Therefore, these equations have been computed for the first time only recently (PAAP and HOMMES,

1984; HÄMMERLI et al, 1987). The simulated formulas are as follows [for the notations, see (5)].

Stator rotating system voltage equation:

$$u_{11} = r_1 i_{11} + l_1 \frac{di_{11}}{dt}$$

$$+ \sum_{\nu} \left\{ \sum_{\lambda_1}^{\infty} \frac{d}{dt}[m'_{21}(\lambda_1) i'_2(\nu) e^{j(\lambda_1-1)p\vartheta}] \right.$$

$$\left. + \sum_{\lambda_1*}^{\infty} \frac{d}{dt}[m'_{21}(\lambda_1*) i'^*_2(\nu) e^{-j(\lambda_1^*-1)p\vartheta}] \right\}$$

$$+ \sum_{\lambda_2}^{\infty} \frac{d}{dt}[m'_{21}(\lambda_2) i'_{2\approx} e^{j(\lambda_2-1)p\vartheta}]$$

$$+ \sum_{\lambda_2*}^{\infty} \frac{d}{dt}[m'_{21}(\lambda_2^*) i'_{2\approx} * e^{-j(\lambda_2*-1)p\vartheta}]. \tag{1}$$

Stator alternating voltage equation:

$$u_{1\approx} = \sum_{\nu} \left\{ \sum_{\lambda_3}^{\infty} \frac{d}{dt}[m'_{2\approx}(\lambda_3) i'_2(\nu) e^{j(\lambda_3-1)p\vartheta} \right.$$

$$\left. + m'_{2\approx}(\lambda_3) i'^{\,*}_2(\nu) e^{-j(\lambda_3-1)p\vartheta}] \right\}$$

$$+ \sum_{\lambda_4}^{\infty} \frac{d}{dt}[m'_{2\approx}(\lambda_4) i'_{2\approx} e^{j(\lambda_4-1)p\vartheta}$$

$$+ m'_{2\approx}(\lambda_4) i'_{2\approx}{}^* e^{-j(\lambda_4-1)p\vartheta}]. \tag{2}$$

Rotor rotating system voltage equation:

$$0 = r'_2(\nu) i'_2(\nu) + l'_2(\nu) \frac{di'_2(\nu)}{dt} - jp\frac{d\vartheta}{dt} l'_2(\nu) i'_2(\nu)$$

$$+ \sum_{\nu_1}^{\infty} \frac{d}{dt}[m'_{12}(\nu_1) i_{11} e^{-j(\nu_1-1)p\vartheta}]$$

$$+ \sum_{\nu_1^*}^{\infty} \frac{d}{dt}[m'_{12}(\nu_1{}^*) i_{11}{}^* e^{j(\nu_1{}^*+1)p\vartheta}]$$

$$- jp\frac{d\vartheta}{dt} \sum_{\nu_1}^{\infty} \frac{d}{dt}[m'_{12}(\nu_1) i_{11} e^{-j(\nu_1-1)p\vartheta}]$$

$$- jp\frac{d\vartheta}{dt} \sum_{\nu_1^*}^{\infty} \frac{d}{dt}[m'_{12}(\nu_1{}^*) i_{11}{}^* e^{j(\nu_1{}^*+1)p\vartheta}]. \tag{3}$$

Rotor alternating system voltage equation:

$$0 = r'_{2\approx}i'_{2\approx} + l'_{2\approx}\frac{di'_{2\approx}}{dt} - jp\frac{d\vartheta}{dt}l'_2(\nu)i'_2(\nu)$$

$$+ \sum_{\nu_2}^{\infty}\frac{d}{dt}[m'_{12}(\nu_2)i_{11}e^{-j(\nu_2-1)p\vartheta} + m'_{12}(\nu_2)i_{11}{}^*e^{j(\nu_2+1)p\vartheta}]$$

$$- jp\frac{d\vartheta}{dt}\sum_{\nu_2}^{\infty}\frac{d}{dt}[m'_{12}(\nu_2)i_{11}e^{-j(\nu_2-1)p\vartheta} + m'_{12}(\nu_2)i_{11}{}^*e^{j(\nu_2+1)p\vartheta}] \qquad (4)$$

Indices of *Eqs. (1)* to *(4)*:

ν $1, 3, 5$ *number of rotor current space harmonics,*

g $0, \pm1, \pm2 \pm 3, \ldots$

h $0, 1, 2, 3, \ldots$

λ_1 $42 \cdot g - (\nu - 1) \cdot 14 + \nu$

λ_1^* $42 \cdot g - (\nu + 1) \cdot 14 + \nu$

λ_2 $42 \cdot g + 7$

λ_2^* $42 \cdot g + 35$

λ_3 $42 \cdot g + 15 \cdot \nu$

λ_4 $42 \cdot g + 42$

ν_1 $42 \cdot g + (\nu - 1) \cdot 14 + \nu$

ν_1^* $42 \cdot g - (\nu + 1) \cdot 14 - \nu$

ν_2 $42 \cdot g + 7$

$$(5)$$

These quite complex equations describe the behaviour of all slots' harmonics in the induction motor. A new method to explain the slots' harmonic equations is to use the aliasing phenomenon for the space distribution of the current in the air gap.

The model assumptions are as follows:

I   The current distribution is constant over the slots' pitch.

II   Beside the slot pitch the current distribution is zero.

III   No saturation is considered.

IV   No current displacement in the stator windings or in the squirrel-cage bars is considered.

Since the motor has two pairs of poles and because of the motor's symmetry just one pole (9 stator slots, 7 rotor slots) needs to be considered to get the whole signal information. The 9 stator slots have distributed windings, and three voltages are externally available (*Fig. 1.*)
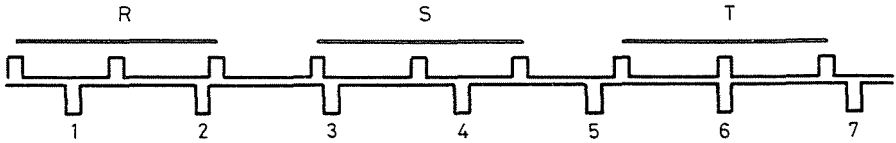
Fig. 1.   The air gap of the considered motor with the slots

Using space vector theory, the spatial current distribution is sampled with 3 space samples on the stator side and with 7 samples on the rotor side. According to the sampling theorem:

$$f_{\text{max detectable}} = 0.5 f_{\text{sampling}}, \tag{6}$$

in the stator windings only one harmonic is detectable (with 3 spatial samples), while the rotor bars detect 3 different space harmonics (with 7 samples). Each space harmonic may have any repetitive current time domain shape, which can be Fourier transformed. Now the formulas (1) to (5) represent the rotor current: (1) and (2), by 3 infinite Fourier Series and the stator current: (3) and (4), by one infinite Fourier Series.

From this complex mathematical model the dominant harmonics only are considered, because the rotor speed is detected using the most dominant harmonic. The model's simulation using (1)–(5) confirmed early investigations (SCHUISKY, 1960, BOEDEFELD, 1971) which had already computed the dominant frequency f_{s1} (7) of the motor in its starpoint voltages:

$$f_{s1} = f_{\text{stator}} + n_{\text{rotor}} \cdot z_{\text{rotor}} \qquad A_{s1} = c \cdot n_{\text{rotor}} \tag{7}$$

where

f_{s1} = Rotor slots harmonics A_{s1} = Amplitude of f_{s1}

z_{rotor} = Number of rotor slots n_{rotor} = Rotor speed.

The amplitude factor c depends on the motor design (air-gap, slot geometry etc).

Due to the reduction of the stator phase voltages, the amplitudes of the rotor slots harmonics decrease if the rotor speed is decreasing (constant nominal motor flux). Beneath 20% of nominal motor speed, the amplitude A_{s1} of the frequency f_{s1} is too small to get a reliable rotor speed signal. Therefore, the inverter's modulator was modified in the following way: For

rotor speeds lower than 30% of nominal speed a three phase 1 kHz sinusoidal signal of constant amplitude is fed additionally to the modulator (*Fig. 2.*). The rotor slots also modulate this 1 kHz signal in correspondence with the normal signal, and the new dominant harmonic frequency f_{s1}^* is computed according to (7), as follows:

$$f_{s1}^* = f_{\text{stator}}^* + n_{\text{rotor}} \cdot z_{\text{rotor}} \qquad (8)$$

where

$$f_{\text{stator}}^* = 1\,\text{kHz additional frequency},$$

$$f_{s1}^* = \text{Dominant rotor slot harmonic}.$$

The advantage of the additional 1 kHz frequency is the constant amplitude of the received dominant rotor slot harmonic f_{s1}^* around 1 kHz. Therefore, it is possible to get a constant signal to noise ratio for small rotor speed.

Modification of the Inverter

The PWM modulator of the inverter was modified to realize the injection method (8) according to *Fig. 2.*
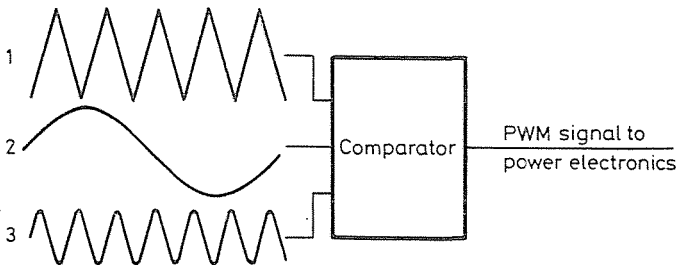
Fig. 2. The PWM Modulator
1 Triangle Signal for PWM (20 kHz)
2 Stator Phase Reference Voltage
3 1 kHz Additional Frequency (to Identify Rotor Speed)

Because of the finite output voltage of the inverter and the operating requirements of the motor, the amplitudes of the three input signals to the modulator are limited. For small rotor speed the motor only needs small driving voltages (law of constant flux) and, therefore, the inverter has a
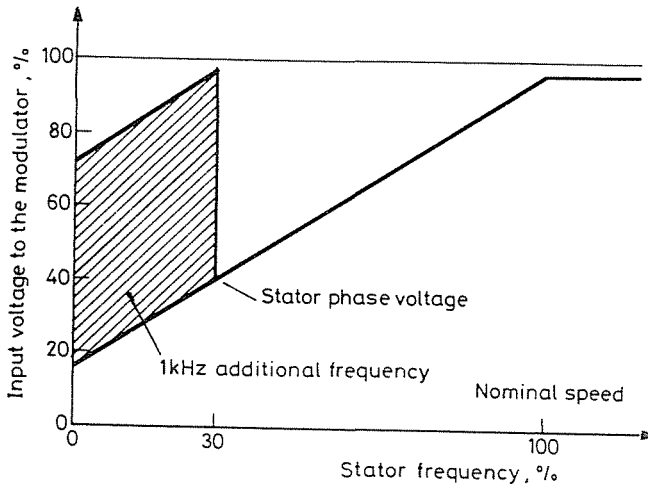
Fig. 3.   Modulator Input Voltages

large unused reserve. The additional 1 kHz signal may be modulated with
remaining amplitude range (more than 50%). Despite the amplitude of the
1 kHz signal, the resulting 1 kHz flux is nearly negligible (<2%) because
of its high frequency. The choice of the modulator's input voltages works
according to *Fig. 3*.

The facts presented above illustrate that only a small change of the
inverter's modulator is used to feed the additional 1 kHz three phase signal
into the motor.

The Detection of Rotor Speed Within Lower Speed Range

The signal to evaluate is measured between the starpoint of the motor and
an artificial starpoint of a 3-R network (*Fig. 4.*). This measuring method
guarantees a very good suppression of all three phase signals and, there-
fore, the rotor slots' harmonics are increased, compared to other harmonics.
According to equation (8) the frequency of the interesting signal f_{s1}^* is in
the range of 790 Hz to 1.21 kHz for a motor with $z_{\text{rotor}} = 28$ slots and an
active injection in the speed range of ±30% of nominal speed. Therefore,
a bandpass filter is used to suppress the 20 kHz clock frequency and the
driving frequency. Then the signal is multiplied by the 1 kHz frequency,
which has the effect of a frequency shift of ±1 kHz. A lowpass filter limits
the signal to approximately 2 kHz. In the next step, the prior knowledge
of rotor speed is used for signal enhancement. Normally the slip of an

asynchronous motor will remain within 10%. From the inverter we know the synchronous frequency (stator frequency) and, therefore, it is possible to add a switched capacitor bandpass filter with a clock frequency proportional to the stator frequency. The output of this filter is converted to a binary signal with a comparator. This output signal has exactly 28 pulses for each revolution. The detector's block diagram is shown in *Fig. 4*.
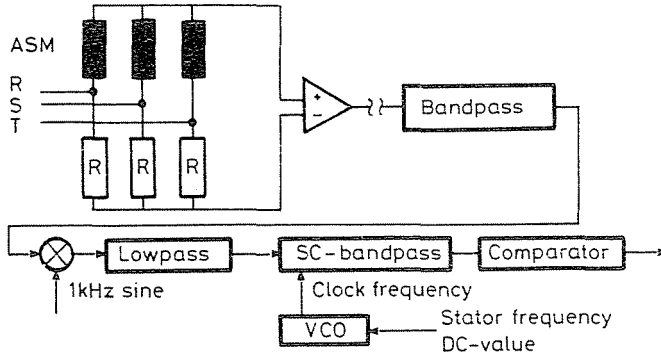
Fig. 4. Block Diagram of the Small Frequency Detector

The Detection of Rotor Speed Within Upper Speed Range

The signal for computing rotor speed within 20% to 100% of nominal rotor speed is also measured between the starpoint of the motor and the artificial starpoint (see *Fig. 4.*). The harmonic of interest, according to equation (7), is between 160 Hz and 750 Hz. The processing of this signal is simpler than the one for small rotor frequencies. First, a bandpass filter is used to enhance the desired frequency range. A comparator transforms the signal to binary pulses. A frequency measurement unit determines from the pulse length the frequency of the binary pulses. From the output frequency the stator frequency is subtracted (according to *Eq.* 7). The signal received depends only of the rotor speed. The block diagram of this process is shown in *Fig. 5*.

Grounding EMC Problems

The inverter used is built with the power transistor BUZ 211, which has a switching slope of 3000 V/μsec and a rise time of about 100 ns. Due to
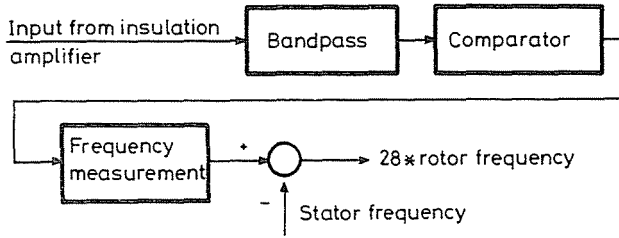
Fig. 5.   Block Diagram of the Normal Range Detector

relation (9) the highest frequency in the PWM signal is 3.3 MHz.

$$f_g * t_r = 1/3 \quad \text{with} \quad t_r = \text{rise time}, \quad f_g \text{the highest frequency.}$$

(9)

The capacitance of the induction motor's winding against the motor's iron is approximately 2.5 nF. For this capacitor follows:

$$f = 20\,\text{kHz} \longrightarrow X_c = 3.2\,\text{k}\Omega, \qquad f = 3.3\,\text{MHz} \longrightarrow X_c = 20\,\Omega.$$

It is understandable that the winding's capacitance has an influence upon the behaviour of the drive. To avoid capacitive currents outside of the motor, e.g. in the electronics of the inverter, the motor must be directly and well grounded. For the electronics of the drive a hierarchical grounding system with a one point connection to earth was applied successfully.

Measurement EMC Problems

The measured voltage is the starpoint voltage of the motor versus a starpoint voltage of an artificial starpoint (*Fig. 4.*), which is discussed in detail in a previous section. This voltage has several characteristic components:
- — A common mode voltage of 20 kHz (carrier of the PWM);
- — A 50 Hz 230 V common mode voltage (the inverter's DC converter is fed directly by a single phase main);
- — A third harmonic voltage, which is produced as a consequence of the iron saturation;
- — The wanted slot harmonic;
- — Noise.

The spectrum of this signal is shown in *Fig. 6.*, in two different frequency scales.
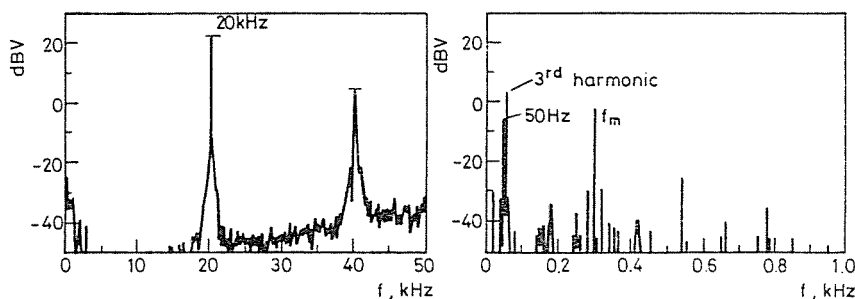
Fig. 6.   Spectrum of the measured voltage (starpoint vs. artificial starpoint)

To measure this voltage, several possible solutions have been investigated. The easiest one is to take an OEM insulation amplifier of adequate performance, which is not acceptable because of the high costs. Therefore, a lot of effort was taken to build a passive filter in the artificial starpoint, to suppress the strong 20 kHz component for decreasing the performance requirements of the instrumentation amplifier. Since the wanted harmonic has a small amplitude, all experiments failed, because the slots' harmonics have quite a high impedance and were, therefore, no longer detectable. Finally, an acceptable solution with BB INA 117 low cost high performance (100 dB common mode rejection at low frequencies) instrumentation amplifier was found.

Frequency Measurement Unit

The frequency measurement unit evaluates the frequency from the pulses of the comparator's output (*Fig. 4.* and *5.*). First the comparator input signal must be considered: it consists of the wanted sinusoidal signal [harmonics in (7) and (8), respectively] distributed by noise. The zero crossings of this signals are varying, therefore, with the noise signal. To improve the frequency measurement, two methods will be discussed.

Method 1 (Frequency averaging)

To decrease the influence of the noise, n frequency results may be averaged. The noise error decreases according to (10) with the square root of the number of pulses $\sqrt{n}$ (a Gaussian distribution of the pulse position on the

time axis with an independent standard deviation σ and a mean value $\mu=0$ is assumed).

$$\sigma_{tot} = \sqrt{\frac{1}{n}\sum_{i=1}^{n}\sigma_i^2} \tag{10}$$

An example is shown in *Fig. 7.* with the following data:

$$T_a \longrightarrow f_1; \quad T_a^* \longrightarrow f_2; \quad f_{res} = 0.5 * (f_1 + f_2); \quad (n = 2)$$

$$\sigma_{tot} = (1/5\sqrt{2}) * \sigma_i.$$

In this example the error σ_{tot} is calculated with a worst-case analysis. The real error σ_{tot} is for this method lower, because the standard deviation σ is not independent. The following calculation shows the effect of the dependent variance.

Each of the positive slopes 1, 2, and 3 (*Fig. 7.*) has an error of $\Delta t_1, \Delta t_2$ and Δt_3, respectively. The frequencies f_1 and f_2 are calculated as follows:

$$f_1 = \frac{1}{T_a(1 + \frac{\Delta t_1}{T_a} + \frac{\Delta t_2}{T_a})}, \quad f_2 = \frac{1}{T_a^*(1 - \frac{\Delta t_2}{T_a^*} + \frac{\Delta t_3}{T_a^*})}.$$

Applying the linearisation of the division for small Δt ($\Delta t \gg T_a$) the result f_{res} (11) is received.

$$\begin{aligned} f_{res} &= \frac{1}{2}\left[\frac{1}{T_a}\left(1 - \frac{\Delta t_1}{T_a} - \frac{\Delta t_2}{T_a}\right) + \frac{1}{T_a^*}\left(1 + \frac{\Delta t_2}{T_a^*} - \frac{\Delta t_3}{T_a^*}\right)\right] \\ &\approx \frac{1}{2}\left[\frac{1}{T_a} + \frac{1}{T_a^*} - \frac{\Delta t_1}{T_a} - \frac{\Delta t_3}{T_a^*}\right] \end{aligned} \tag{11}$$

where $T_a \approx T_a^*$.

As (11) shows, the error due to the noise is decreasing with the number of averaged frequencies n. It is, therefore, supposed that this method is nearly as good as the next method.

Method 2 (Time prolongation)

To decrease the influence of the noise on the frequency result, the frequency may be measured within n pulses, instead of one. The result improves with the number of the pulses n.

Possible range of the signal according to the noise disturbance
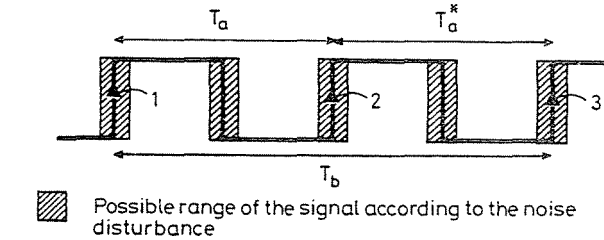
Fig. 7. Frequency evaluation of the comparator's output
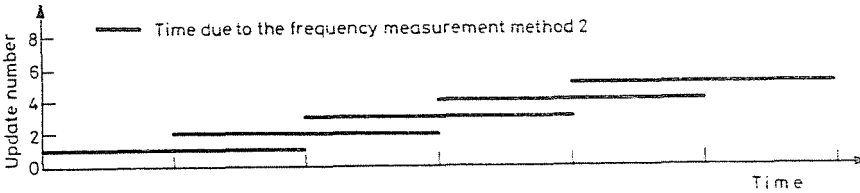
Fig. 8. Overlapping method to improve update time

An example is shown in *Fig. 7.* with the following data:

$$T_b \longrightarrow f_{res}; \quad (n = 2)$$

$$\sigma_{tot} = (1/2) * \sigma_{:}.$$

Method 2 has the disadvantage of a longer updating time of the frequency information. An overlapping observation time method improves the result (*Fig. 8.*).

With this overlapping method the disadvantage of a slower updating of method 2 is eliminated.

Displaying the Rotor Speed

A TMS 9995 microcomputer system displays the rotor speed on an LCD. The pulse frequencies from the two detectors are measured in a peripheral chip. As explained above, both detectors are active in the range of 20% to 30% of nominal rotor speed. The processor decides, using some hysteresis, which one of the results in the mentioned range has to be displayed.

Conclusions

The presented detector has been realised in a laboratory version and works in the range of 2% to 100% of nominal rotor speed, as well as in the range of field weakening (more than nominal rotor speed). The hardware, without the CPU cards needed in this application, consists of two euro-boards of low cost electronics.

The reached accuracy is comparable to that achieved using a usual tachogenerator.

References

BOEDEFELD, Th. (1971): Elektrische Maschinen. (Electrical Machines). Springer. (In German)

FRANZ, P. (1974): Zur Dynamik von Drehstrom-Asynchronmotoren mit Käfigläufer unter Berücksichtigung der Oberfelder und der Streufeldsättigung. (On the Dynamics of Three Phase Squirrel Cage Induction Motors, with emphasis on the Spacial Harmonics and Saturation of Induction loss.) Dissertation TU München. (In German)

HÄMMERLI, B. (1986): Rotor Speed Detector for Induction Machines Utilizing Rotor Slots Harmonics. *Proceedings of the International Conference on Evolution and Modern Aspects of Induction Machines.* Torino, Italy. pp. 352–354.

HÄMMERLI, B. – TANNER, R. – ZWICKY, R. (1987): A Rotor Speed Detector for Induction Machines Utilizing Rotor Slots Harmonics and an Active Three Phase Injection. *Proceedings of the Second European Conference on Power Electronics and Application (EPE),* Grenoble, France, September 22–24, Vol. 2, pp. 599–604.

ISHIDA, M. – IWATA, K. (1984): A New Slip Frequency Detector of an Induction Motor Utilizing Rotor Slots Harmonics. *IEEE Transactions on Industry Application,* Vol. IA-20, No. 3, May/June, pp. 572–583.

PAAP, G. – HOMMES, E. (1984): The Analysis of the Squirrel-Cage Induction Motor with Space Harmonics. *Archiv für Elektrotechnik,* Vol. 67, pp. 217–236.

SCHUISKY, W. (1960): Berechnung Maschinen. (Calculating Machines.) Heidelberg, Springer. (In German)

TAEGEN, F. – HOMMES, E. (1972): Das allgemeine Gleichungssystem des Käfigläufermotors unter Berücksichtigung der Oberfelder. (The General Equations representing the Squirrel Cage Induction Motor with its Spacial Harmonics.) *Archiv für Elektrotechnik,* Vol. 55, pp. 21–31 and pp. 98–105. (In German)

Addresses:

Dr. Bernhard HÄMMERLI
CH-5430 Wettingen, Mooshaldestr. 15.
Switzerland

Prof. Dr. Rudolf ZWICKY
CH-8092 Zürich, ETH-Zentrum
Switzerland